AGU PUBLICATIONS

JGR

Journal of Geophysical Research: Oceans

RESEARCH ARTICLE

10.1002/2015JC010912

Observed ocean thermal response to Hurricanes Gustav and Ike

Patrick C. Meyers[1], Lynn K. Shay[2], Jodi K. Brewster[2], and Benjamin Jaimes[2]

[1]Cooperative Institute for Climate and Satellites, Earth System Science Interdisciplinary Center, University of Maryland, College Park, Maryland, USA, [2]Department of Ocean Sciences, Rosenstiel School of Marine and Atmospheric Science, University of Miami, Miami, Florida, USA

Key Points:
- Ocean response to two hurricanes were observed during a 2008 field campaign
- Satellite methods accurately measured prestorm ocean heat content
- The near-inertial response could not be captured by the two-layer model

Correspondence to:
P. C. Meyers,
pmeyers@umd.edu

Citation:
Meyers, P. C., L. K. Shay, J. K. Brewster, and B. Jaimes (2016), Observed ocean thermal response to Hurricanes Gustav and Ike, *J. Geophys. Res. Oceans*, *121*, 162–179, doi:10.1002/2015JC010912.

Received 16 APR 2015
Accepted 2 DEC 2015
Accepted article online 9 DEC 2015
Published online 10 JAN 2016

Abstract The 2008 Atlantic hurricane season featured two hurricanes, Gustav and Ike, crossing the Gulf of Mexico (GOM) within a 2 week period. Over 400 airborne expendable bathythermographs (AXBTs) were deployed in a GOM field campaign before, during, and after the passage of Gustav and Ike to measure the evolving upper ocean thermal structure. AXBT and drifter deployments specifically targeted the Loop Current (LC) complex, which was undergoing an eddy-shedding event during the field campaign. Hurricane Gustav forced a 50 m deepening of the ocean mixed layer (OML), dramatically altering the prestorm ocean conditions for Hurricane Ike. Wind-forced entrainment of colder thermocline water into the OML caused sea surface temperatures to cool by over 5°C in GOM common water, but only 1–2°C in the LC complex. Ekman pumping and a near-inertial wake were identified by fluctuations in the 20°C isotherm field observed by AXBTs and drifters following Hurricane Ike. Satellite estimates of the 20° and 26°C isotherm depths and ocean heat content were derived using a two-layer model driven by sea surface height anomalies. Generally, the satellite estimates correctly characterized prestorm conditions, but the two-layer model inherently could not resolve wind-forced mixing of the OML. This study highlights the importance of a coordinated satellite and in situ measurement strategy to accurately characterize the ocean state before, during, and after hurricane passage, particularly in the case of two consecutive storms traveling through the same domain.

1. Introduction

Tropical cyclones (TC) are some of the strongest forcing events to the ocean. Winds create intense currents in the ocean mixed layer (OML), force mixing events and entrainment of colder thermocline waters at the base of the OML, and cause upwelling of thermocline water by Ekman pumping [*D'Asaro*, 1985; *Jacob et al*., 2000]. The magnitude of the currents and sea surface temperature (SST) cooling due to mixing and entrainment is partly tied to the thermal structure of the ocean lying beneath the TC. These ocean parameters affect the air-sea interaction and the enthalpy fluxes of heat and moisture at the surface, directly impacting storm intensity. Thus, it is necessary to understand the ocean's thermal and kinematic response to TC passage to improve forecasting of both systems.

The OML is homogeneous, with minimal density stratification with depth. Currents in the OML generate shear across the OML base, which can cause entrainment of cooler thermocline waters by eroding away the top of the thermocline. This acts to deepen the OML with two important consequences: (i) the wind-driven transport reduces velocity because it is spread over a deeper layer, and (ii) SSTs decrease because of the cool water entrainment [*Sanford et al*., 1987; *Shay et al*., 1992]. If cold water is near the surface (i.e., the OML is shallow), then any mixing will create a greater amount of cooling in the OML. Reducing SSTs during TC passage inhibits latent and sensible heat fluxes across the air-sea interface into the hurricane boundary layer. Therefore, accurately diagnosing the SST and underlying OML responses are central to understanding TC intensity fluctuations.

The oceanic energy source for TCs has long been known to be related to SST [*Palmen*, 1948; *Fisher*, 1958]. *Leipper* [1967] introduced the concept of Ocean Heat Content (OHC) as a quantity of thermal energy in the ocean above the minimum threshold for TC formation, assumed to be 26°C [*Palmen*, 1948].

$$OHC = \int_{D26}^{Sfc} c_P \rho (T - 26^{\circ}\mathrm{C})\, dz \tag{1}$$

where c_p is the specific heat of seawater, ρ is the density of water, and T is temperature. OHC quantifies the amount of thermal energy potentially available to storms in the upper ocean. OHC is directly related to the

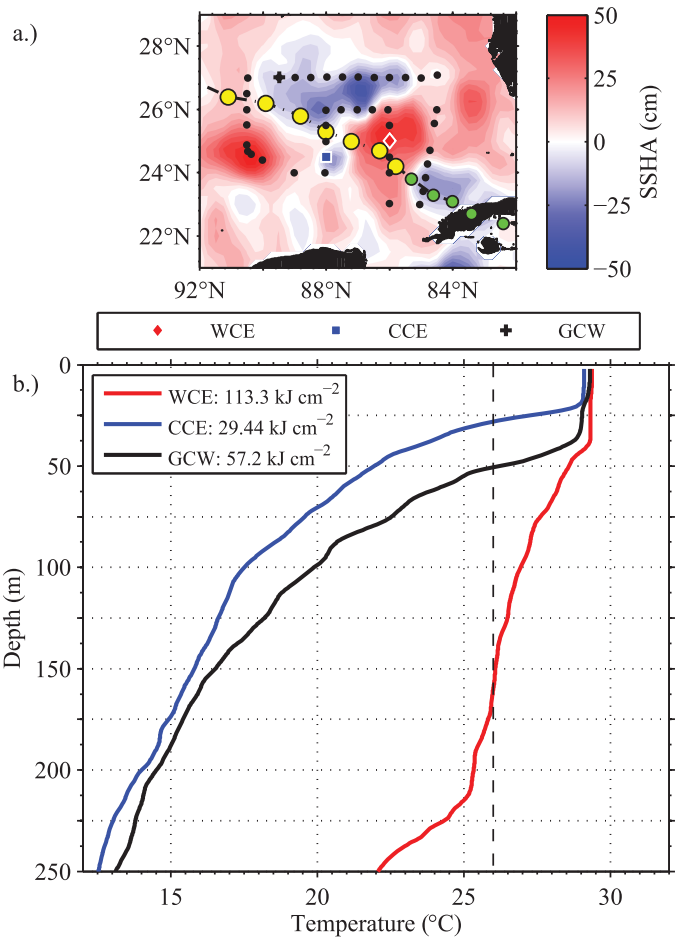

Figure 1. (a) SSHA field prior to Hurricane Ike on 8 September with the locations of AXBT deployments. (b.) Profiles of GCW (black), WCE (red), and CCE (blue) identified by corresponding symbols in Figure 1a. SSTs are similar between profiles, however OHC varies greatly.

persistent mixed layer depth (MLD), depth of the 26°C isotherm (D26), and SST, such that thick layers of warm water (deep MLD and D26 and warm SST) are the most favorable for TC growth.

The Gulf of Mexico (GOM) is of particular interest for hurricane intensity forecasting, due to its complex oceanographic features and high number of coastal communities vulnerable to hurricane landfall. The most notable ocean features in the GOM that can affect hurricane intensity are the warm core eddies (WCEs) that are shed from the Loop Current (LC). WCEs are characterized by deep OMLs and a weakly stratified thermocline, which support high OHC relative to the surrounding Gulf Common Water (GCW). During a WCE shedding event, oppositely rotating cold core eddies (CCE) are often found along the perimeter of the LC. The WCE/LC, CCE, and GCW have unique temperature structures (Figure 1). Several case studies have shown the importance of OHC in the rapid intensification of TCs over WCEs [e.g., *Emanuel*, 1999; *Shay et al.*, 2000; *Lin et al.*, 2005; *Wada and Chan*, 2008; *Jaimes and Shay*, 2009; *Jaimes et al.*, 2015]. The reduction of the negative intensity feedback mechanism over WCEs can maintain heat and moisture fluxes across the air-sea interface. *Mainelli et al.* [2008] found using OHC as a predictor of intensity in the Statistical Hurricane Intensity Prediction Scheme improved forecasting of intensity of Category 5 storms by 5–6% on average, and by as much as 20% during Hurricane Ivan's passage in 2004.

For this reason, the initial state of the ocean must be known to make the most accurate hurricane forecasts [*Halliwell et al.*, 2008; *Shay and Uhlhorn*, 2008]. Mesoscale ocean features (including WCEs) are often measured with in situ temperature profile measurements, as well as a satellite estimate using sea surface height anomalies (SSHA) [*Meyers et al.*, 2014]. Airborne oceanography flights typically target regions of high eddy variability and locations of anomalously high or low sea surface heights measured by satellites. These locations correspond to points where the depth of the 20°C isotherm (D20), D26, and OHC are significantly different than their climatological values.

The goal of this study is to quantify the observed upper ocean cooling and deepening of the OML during a 2008 field campaign, as well as to determine if satellite-derived estimates were able to resolve large changes in ocean thermal structure after major wind-forcing events. The field campaign is described in section 2. The in situ measurements and satellite estimation methodology are explained in section 3. Section 4 describes the observed changes to the in situ and satellite data fields after TC passage. The forced and relaxation stages of the ocean response are described in section 5. Section 6 discusses the results, and a summary is provided in section 7.

Table 1. Deployment of AXBTs for Hurricanes Gustav and Ike[a]

	Gustav			Ike	
Date	Flight	AXBT	Date	Flight	AXBT
28 Aug	RF43	49(2)	08 Sep	RF43	47(2)
29 Aug	RF42	16(0)	09 Sep	RF42	6(0)
30 Aug	RF43	19(2)	10 Sep	RF43	20(7)
31 Aug	RF43	19(1)	10 Sep	RF42	10(2)
31 Aug	RF42	16(1)	11 Sep	RF43	22(3)
01 Sep	RF43	19(0)	11 Sep	RF42	10(1)
03 Sep	RF43	54(4)	12 Sep	RF43	20(4)
			12 Sep	RF42	10(4)
			15 Sep	RF43	61(5)
Total	7	191(10)		9	216(28)

[a]A pre and poststorm array was deployed along the hurricane track and in-storm AXBTs were launched in hurricane conditions. Total number of probes for each flight is listed, with failures in parentheses.

2. 2008 Hurricane Season Field Experiment

In collaboration with NOAA's Hurricane Research Division (HRD) and Aircraft Operation Center, 407 AXBTs were deployed from WP-3D aircraft as part of a field campaign to simultaneously observe the hurricane atmospheric boundary layer and upper ocean temperature field over the life cycles of Gustav and Ike (Table 1 and Figure 2). Prior to the passage of both hurricanes, an array of AXBTs was deployed along the forecasted path of the storm. During in-storm flights, AXBTs and GPS radiosondes were launched during transects through the hurricane in a "figure 4" pattern. After landfall, an array of AXBTs was deployed in cross sections along the storm track. With observations before, during, and after the storm, the impacts of the storm-induced cooling and deepening of the OML could be examined spatially.

During the lifetimes of Gustav and Ike, a WCE was in the process of shedding from the LC. Over the course of the few weeks surrounding the two storms, a large intrusion of the LC began to break off to create the foundation of a WCE. Both Gustav and Ike traveled over the WCE after crossing Cuba and entering the GOM. These storms did not undergo rapid intensification above the WCE due to synoptic scale atmospheric conditions. Hurricane Gustav's development was inhibited by dry air entrainment associated with an upper level high pressure ridge [*Beven and Kimberlain*, 2009]. Over the LC complex, Hurricane Ike underwent an eyewall replacement cycle which caused maximum wind speed to decline. Despite the decrease in maximum wind speed, eyewall replacement cycles increase the storm's total kinetic energy due to the new eyewall's larger area [*Maclay et al*., 2008].

2.1. Storm History

The TC track, speed, and wind field characteristics force the horizontal motion and vertical mixing of the ocean. An accurate record of TC track and winds is necessary to understand the complex interactions at the air-sea interface. TC track and intensity information was extracted from the National Hurricane Center's HURDAT2 database [*Landsea and Franklin*, 2013]. Instantaneous wind field data and total kinetic energy was supplied by the HRD's H*Wind analysis [*Powell et al*., 1998].

2.1.1. Hurricane Gustav

Hurricane Gustav developed from a tropical wave during a period of increased wave generation near Cape Verde. Gustav was briefly a Category 1 hurricane prior to landfall in Haiti on 26 August 2008. Gustav traveled westward through the Caribbean as a tropical storm due to topographical effects from Hispaniola and an upper level atmospheric ridge over Florida. Deep warm Caribbean waters and favorable atmospheric conditions sparked rapid deepening, intensifying Gustav from a tropical storm to a major hurricane in 24 h. As a Category 4 hurricane, Gustav made landfall in western Cuba on 30 August 2008. The storm subsequently emerged to the north of Cuba on 31 August 2008, maintaining its Category 4 status. An upper level ridge, as well as dry air entrainment caused Gustav to weaken over the GOM over the next 2 days, while quickly traversing a WCE. Although maximum wind speed weakened, Gustav's wind field expanded horizontally over the GOM, with tropical storm force winds extending over 200 nm from the storm's center. Gustav eventually made landfall near Cocodrie, LA on 1 September 2008 as a Category 2 hurricane and rapidly weakened as the storm's remnants traveled north to the Great Lakes [*Beven and Kimberlain*, 2009].

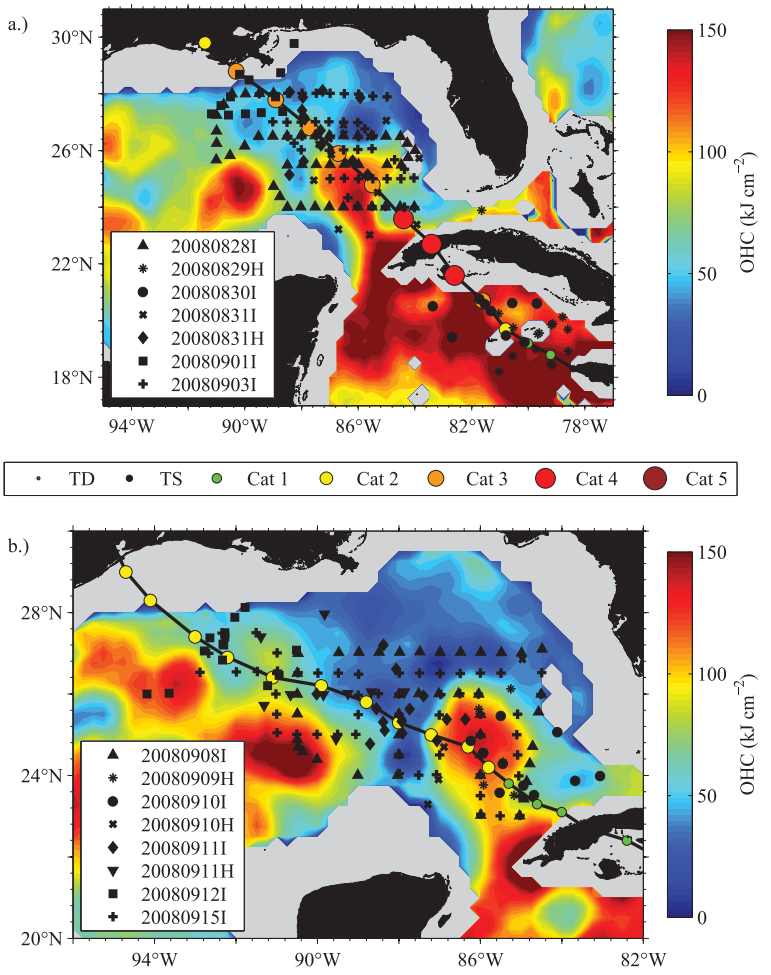

Figure 2. Locations of AXBTs launched during the 2008 hurricane season for Hurricanes (a) Gustav and (b) Ike. Drop locations are layered over satellite-derived OHC.

2.1.2. Hurricane Ike

Hurricane Ike reached major hurricane status on 4 September 2008 when the storm was well east of the Caribbean. Eastern Cuba received the brunt of the hurricane force winds when Ike made landfall as a Category 4 hurricane on 8 September 2008. The storm weakened as it traveled westward over Cuba until its eye emerged just to the south of the island. Although Ike was centered over the Caribbean Sea, its interaction with the Cuban landmass disturbed the inner core dynamics, limiting future organization and intensification. Ike crossed Cuba to the northwest and into the GOM on 10 September 2008. Once over the GOM, the storm passed south of the LC bulge, and Ike intensified from a Category 1 to Category 2 storm (Figure 1b). However, an eyewall replacement cycle limited the storm's ability to rapidly intensify due to angular momentum constraints. Weak inner-core convection and an expansive wind field also limited Ike's intensification [*Berg*, 2009]. Ike made landfall as a Category 2 hurricane on 12 September 2008 just north of Galveston, TX, bringing with it a large storm surge that inundated many coastal communities.

While maximum wind speeds from H*wind suggest Ike was less powerful than Gustav, Ike had a massive wind field of TS force winds. While over the LC/WCE, Gustav had an integrated kinetic energy of TS force winds of 63.1 TJ (1 TJ = 10^{12} J) (1330 UTC 31 August), whereas Ike was 5 m s^{-1} weaker but had an integrated KE of 149 TJ (1930 UTC 10 September). Such a large wind field had a dramatic effect on the ocean SSTs and thermal structure and its storm surge at landfall.

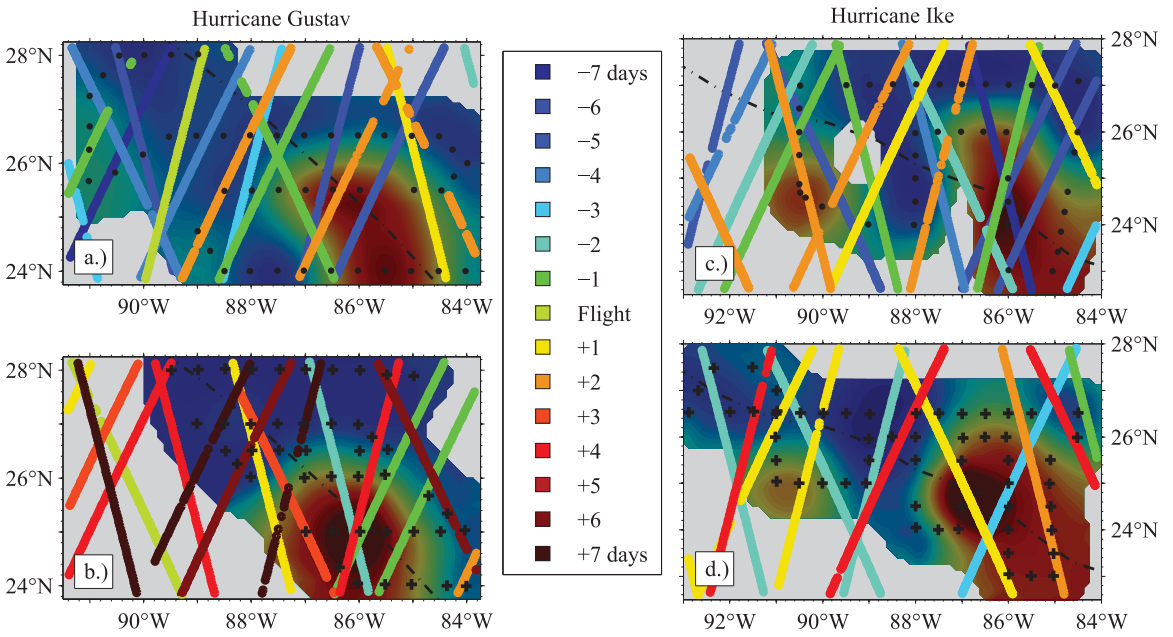

Figure 3. Available altimeter tracks in a 10 day window (a) before (28 August) and (b) after (3 September) passage of Hurricane Gustav, as well as (c) before (8 September) and (d) after (15 September) passage of Hurricane Ike. The typical ±5 day observation window is offset to ensure only SSHAs from before and after hurricane passage are used for pre and poststorm analysis, respectively. Tracks are overlaid on AXBT observed D20 for the day of the flight. The color of the track represents the time of SSHA observation relative to the date of airborne reconnaissance.

3. Data

Coordinated in situ and satellite measurements provide the best characterization of the three-dimensional ocean state. In situ measurements provide the highest quality data with the greatest accuracy; however, field campaigns can undersample regions of interest in time and space. Satellite measurements provide near-global coverage, but are more prone to accuracy errors. Additionally, in situ observations are critical to validate the satellite retrievals.

3.1. In Situ Profiles

Mesoscale and synoptic scale ocean observations can be collected using expendable probes launched from airborne platforms. AXBTs are often launched by NOAA WP-3D aircraft during TC reconnaissance and research flights. As the payload descends through the water column, it transmits data to a digital recorder on the aircraft, where the signal is converted into a temperature estimate accurate to ±0.2°C. Depth is estimated using a known time-depth relationship accurate to ±2% [*Boyd*, 1987].

Airborne expendable data used in this study were processed and quality controlled by University of Miami's Upper Ocean Dynamics Laboratory [*Shay et al.*, 2011]. Each raw profile was passed through a nine element median filter twice to remove errant data. The profile was then visually inspected to remove any remaining noise and then compared to surrounding profiles. Any questionable or excessively noisy profiles were removed from the data set.

Additionally, an array of nine drifters was deployed perpendicular to the forecasted tracks of Hurricanes Gustav and Ike as part of the Atlantic Oceanographic and Meteorological Laboratory's Global Drifter Program. Each drifter was equipped with a series of thermistors to measure hourly changes in upper ocean temperature structure down to 150 m.

3.2. Satellite Thermal Structure Estimates

The two-layer reduced gravity model used to estimate D20, D26, MLD, and OHC in the North Atlantic hurricane basin from satellite-measured SST and SSHA is described in detail in *Meyers et al.* [2014]. The model assumed two layers of constant density separated by D20, which typically occurred within the thermocline. Objective analysis (OA) of 10 days of SSHAs measured by Jason-1, GFO, and Envisat forced the 1-D two-layer model [*Mariano and Brown*, 1992]. Positive (negative) SSHAs corresponded to a deepening (shoaling) of

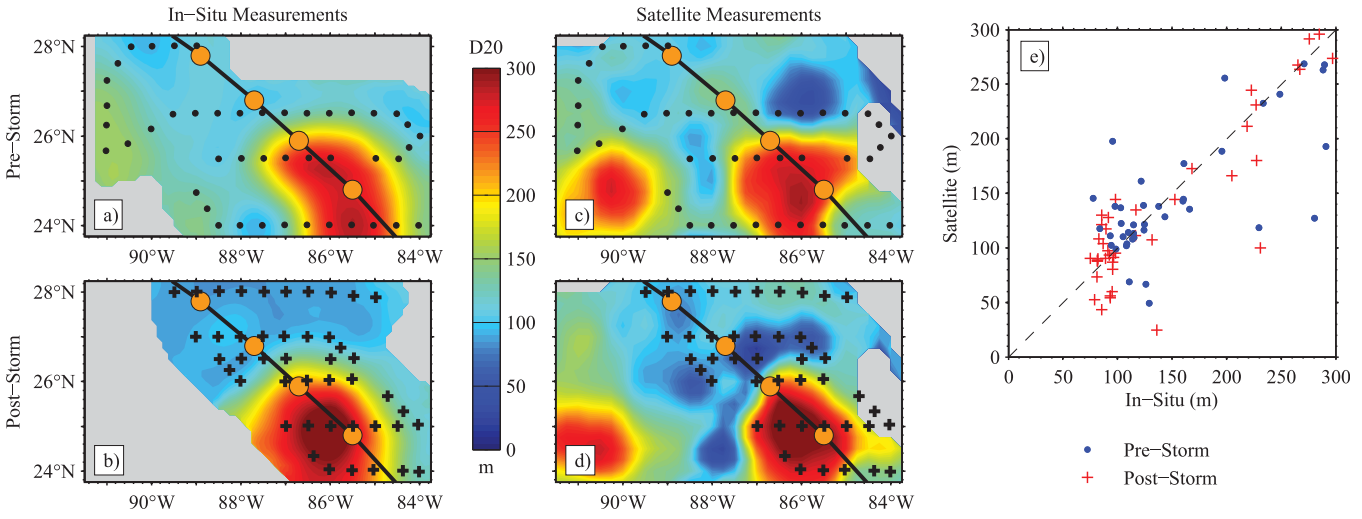

Figure 4. Observations of D20 for Hurricane Gustav. (a) In situ prestorm. (b) In situ post-storm. (c) Satellite prestorm. (d) Satellite poststorm. (e) Scatterplot of in situ D20 measurements compared to satellite-derived values for prestorm (blue dot) and poststorm (red +). Observations were taken on 28 August and 3 September for prestorm and poststorm conditions, respectively.

D20 relative to its climatological depth. Uniform stretching of the climatological temperature profile was assumed, such that the climatological ratios of D20 to MLD and D26 were preserved. Daily climatological values of D20, D26, MLD, and reduced gravity were extracted on a 0.25° grid from the Systematically Merged Regional Atlantic Temperature and Salinity Climatology (SMARTS) [*Meyers et al.*, 2014]. The model is summarized by these equations:

$$\boldsymbol{D20} = \overline{\boldsymbol{D20}} + \frac{\overline{\rho}_2}{\overline{\rho}_2 - \overline{\rho}_1}\eta' \tag{2a}$$

$$\boldsymbol{D26} = \frac{\overline{\boldsymbol{D26}}}{\overline{\boldsymbol{D20}}}\boldsymbol{D20} \tag{2b}$$

$$\boldsymbol{MLD} = \frac{\overline{\boldsymbol{MLD}}}{\overline{\boldsymbol{D20}}}\boldsymbol{D20} \tag{2c}$$

D20 is modified by the SSHA (η') and the reduced gravity term calculated from the densities of the upper and lower layers, ρ_1 and ρ_2, respectively. The overbar denotes the SMARTS climatological value of a parameter.

The resultant satellite-estimated upper ocean temperature profile has an OML with a constant temperature from Remote Sensing Systems' Optimally Interpolated SST product [*Gentemann et al.*, 2004]. A constant vertical temperature gradient is assumed from the bottom of the OML to D26. The OHC integration in equation (1) of the satellite-derived profile simplifies to the area of a right trapezoid with a height of (SST: 26°C) and bases MLD and D26.

$$\boldsymbol{OHC} = \frac{1}{2}\boldsymbol{\rho_1 c_P}(\boldsymbol{D26} + \boldsymbol{MLD})(\boldsymbol{SST} - \boldsymbol{26}^{\circ}\mathrm{C}) \tag{3}$$

It should be noted that the SST product removes the effects of diurnal heating [*Gentemann et al.*, 2003], and the shallow daytime near-surface mixed layer is omitted. Over the entire North Atlantic hurricane basin, the root mean square difference (RMSD) between in situ profiles for D20, D26, and OHC were 31.0 m, 18.2 m, and 15.0 kJ cm^{-1}, respectively. RMSD values in the LC and GOM were higher (41.9 m, 24.5m, and 26.1 kJ cm^{-1}) due to the higher average values and greater spatial and temporal variability of the parameters [*Meyers et al.*, 2014].

3.3. Daily Altimetry Data From 10 Day Composites

Typically, a 10 day composite of SSHA observations centered on the day of interest is used to determine the daily SSHA field. TCs induce changes to SSHA [*Shay et al.*, 1990], making it necessary to shift the 10 day

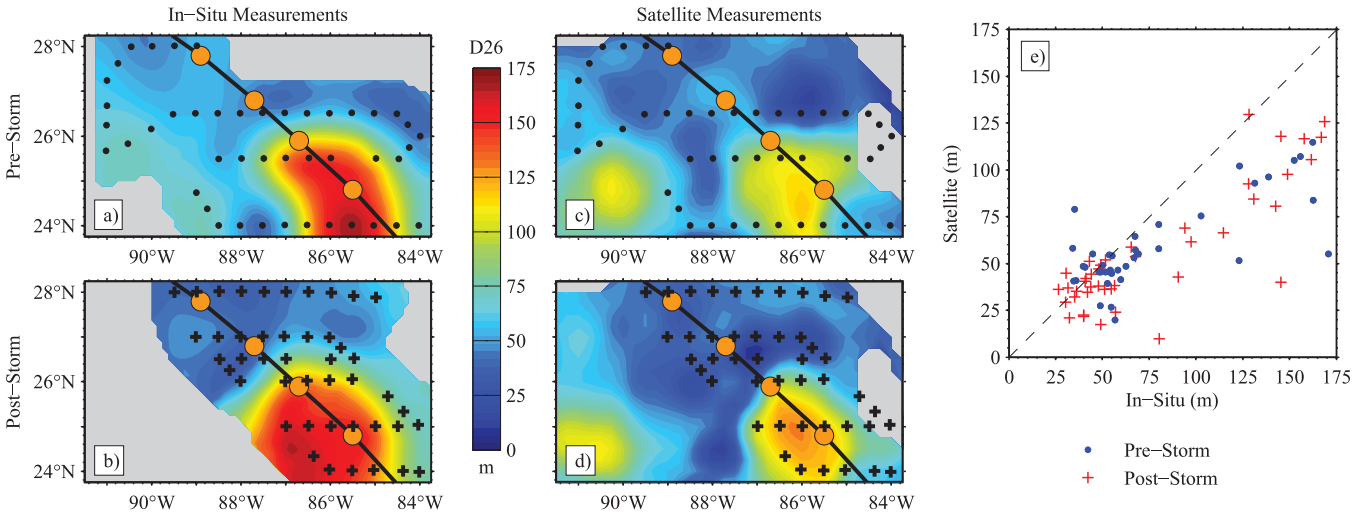

Figure 5. Same as Figure 4, but D26.

observational window such that SSHA data observed after (before) storm passage was not used for the prestorm (poststorm) data set. Maintaining a 10 day window of SSHA data ensured full basin coverage by the 10 day altimeter. Satellite SST estimates from the day of AXBT deployment provided the surface conditions for the OHC calculation.

The LC core fell in the observational gap prior to Hurricane Gustav, although the western and northern fronts of the LC were sampled by altimeters (Figure 3a). The CCE to the west of the LC/WCE complex was not observed by a direct overpass, but the region of shallow thermocline depths directly to the north was thoroughly covered. In the days following Gustav's passage, several altimeter tracks passed over the LC region. The CCE to the northwest was observed over a week after hurricane passage (Figure 3b).

Due to the quick succession of the two storms, the same altimetry data were used to estimate the post-Gustav and pre-Ike fields (Figures 3b and 3c). The satellite OHC estimates during these two deployments were not identical because of the daily SST fields and the propagation of SSHA features calculated in the OA technique. The pre-Ike AXBT array was well covered by altimeters, although the core of the CCE west of the LC was not directly sampled. SSHA data were sparser for the post-Ike array, with a lack of altimetry data in the CCE west of the LC and the northern frontal region of the LC/WCE complex. The western WCE and the northern CCE regions were well covered by altimetry in both pre and poststorm flights.

4. Observed Ocean Thermal Structure Changes

4.1. Hurricane Gustav

4.1.1. In Situ Observations

Prior to Hurricane Gustav's emergence over the GOM, 49 AXBTs were deployed on 28 August 2008 in a "lawn mower" pattern transecting the LC and frontal region three times prior to sampling an area where satellite altimetry identified a mature WCE and CCE (Figure 1a). At this time, the LC protruded NNW with the frontal region extending to 26°N with a slight westward hook due to CCEs located to the west (CCE_W) and north (CCE_N). The AXBT observations did not suggest that a WCE had been shed from the LC, with maximum observed D20 (D26) values of 290 m (160 m) along both transects through the LC (Figures 4a and 5a). Outside of the LC/WCE, temperature profiles indicated a shallow OML above a strongly stratified thermocline which weakened with depth, and D26 was only 35m in CCE_W. Despite the variability of subsurface temperature, SSTs only ranged from 29.2 to 30.5°C (Figure 7a).

Hurricane Gustav crossed directly over the LC as a Category 3 storm. Poststorm observations suggested that the eddy began to detach from the LC. A local D20 maximum near (86°W, 25°N) identified a closed eddy circulation embedded in the northward extension of the LC (Figure 4b), likely due to eddy intensification similar to that caused by Hurricanes Rita [*Jaimes and Shay*, 2009] and Isaac [*Jaimes and Shay*, 2015] over the LC

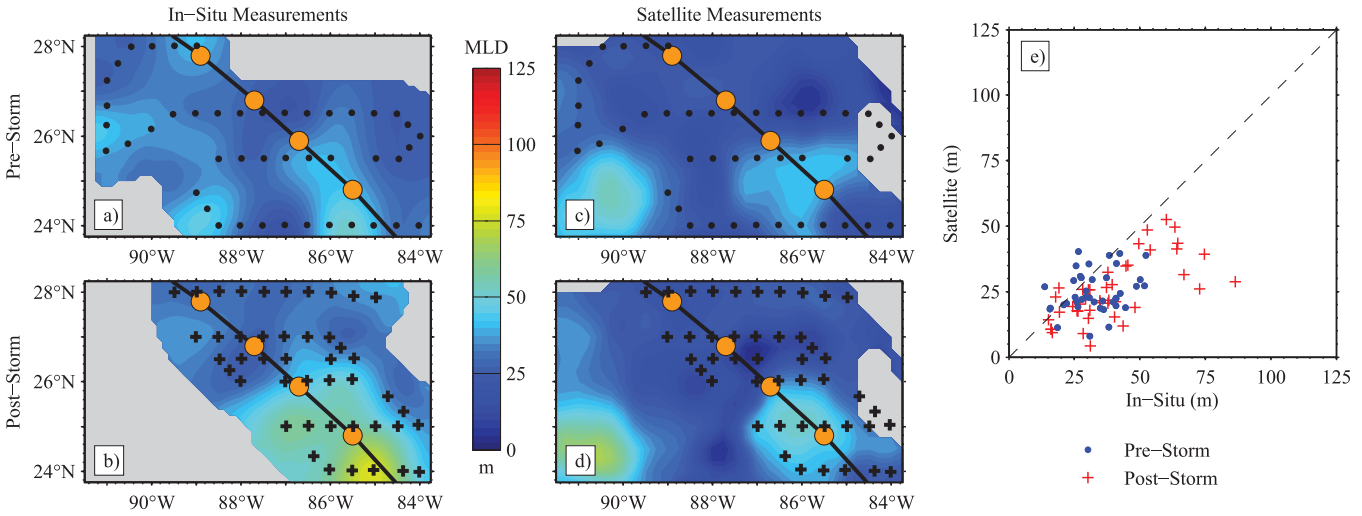

Figure 6. Same as Figure 4, but MLD.

eddy field. This closed circulation was not identifiable in the D26 observations (Figure 5b). To the south of the eddy, observations showed the LC maximum depths shift 50 km westward.

In areas with AXBTs collocated in the pre and poststorm flights, the direct impacts of Gustav on the ocean could be examined. Maximum winds speeds over the LC were 50 m s^{-1} in Gustav's northwest quadrant on 31 August 2008. Temporal changes of D20 and D26 in the LC showed the westward migration of the WCE as it separated from the LC. Beneath the storm center, some shoaling of deeper waters was expected due to Ekman pumping [*Gill*, 1984]. Scale analysis estimated isotherm displacement forced by Ekman pumping ($L = \tau/\rho fU$) on the order of 15 m [*Price*, 1983], which was consistent with ~20 m upwelling of D20 and D26 observed after Gustav's passage over the WCE (Figure 5b). A near-inertial response was also observed in the storm's wake, which also contributed to deviations from the prestorm ocean state, as discussed in section 5. Wind-forced mixing induced deepening of the LC OML by up to 40 m underneath the storm track (Figure 6b). In this region, the upper ocean is weakly stratified, such that wind or buoyancy forcing can cause relatively large deepening of the OML. In the LC/WCE complex, SSTs decreased by only 0.5–1.0°C (Figure 7b). Despite the SST cooling, OHC values to the west of the WCE increased due to its westward propagation (Figure 8b). The largest SST decrease occurred to the north of the observed array along the east side of the

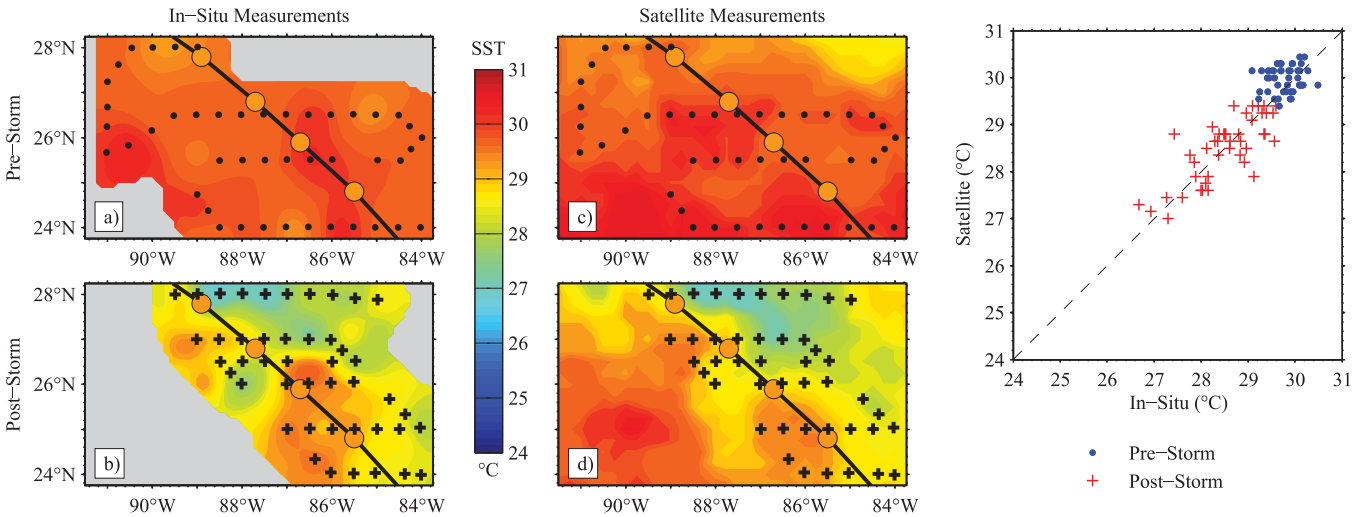

Figure 7. Same as Figure 4, but SST.

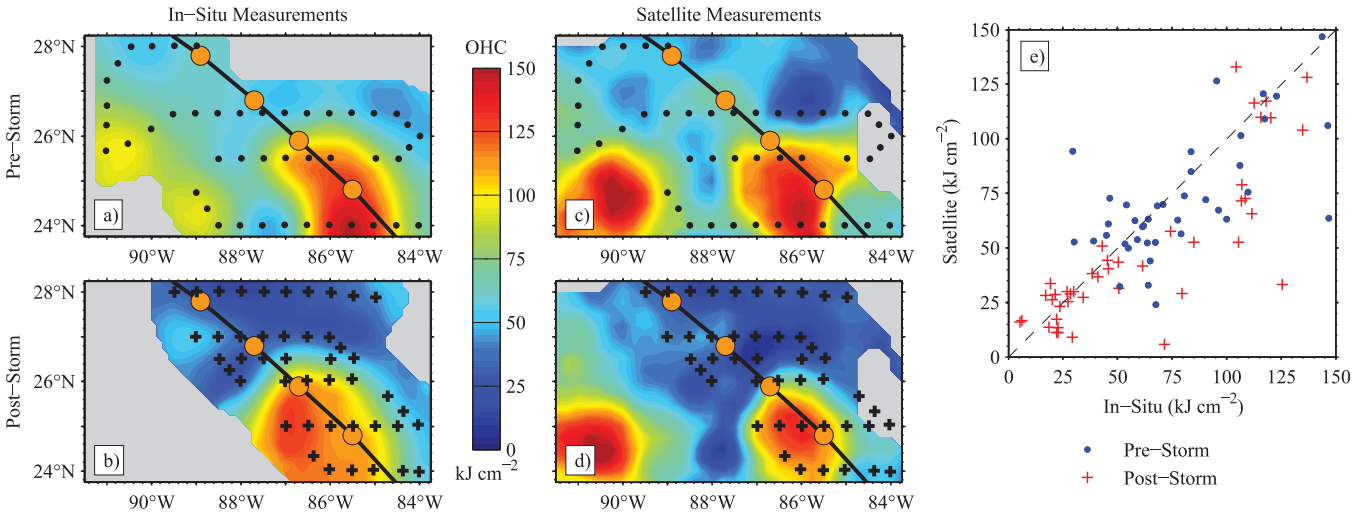

Figure 8. Same as Figure 4, but OHC.

storm track. Assuming SSTs were relatively uniform over the entire GOM prior to Gustav, SSTs decreased by as much as 2.5°C in the northern region.

4.1.2. Satellite Estimations

The prestorm estimations of D20 were accurate and comparable to in situ observations (Figures 4a and 4c). The maximum D20 isotherm depth in the core of the LC/WCE complex was observed and estimated to be near 280 m, despite poor coverage by altimeters (Figure 3a). Satellite estimations accurately identified the location of the western LC frontal region along AXBT transects at 24.0° and 25.5°N; however, a large region of negative SSHAs in the southeast of the array caused a large underestimation of D20 and D26 near the eastern extent of the LC (Figures 4e and 5e). The northern front of the LC/WCE complex was accurately located and a SSHA minimum to the north suggested a sharper horizontal gradient relative to in situ observations. The satellite observations identified the CCE_N which was not resolved by the AXBT sampling, leading to a weaker D20 gradient in the in situ observations. In the CCE_W, D20 was underestimated by 20 m, although this may be attributed to OA extrapolation.

Despite the accuracy of D20, satellite estimations of the D26 isotherm surface in the LC/WCE complex were underestimated due to a departure from the climatological $\overline{D26/D20}$ ratio (Figure 5c, equation (2b)). In the core of the LC, the observed $\overline{D26/D20}$ ratio was near 0.55, larger than the ~0.4 ratio in SMARTS [*Meyers*, 2011]. Comparisons to data from other hurricane seasons showed that the observed ratio in 2008 was much larger than other years, such that the 0.4 climatological ratio was reasonable for future calculations. AXBT profiles in the LC contained a weakly stratified layer below the OML with a temperature just above 26°C, causing large satellite underestimations of the D26 isotherm while not contributing greatly to the in situ value of OHC (Figures 5c and 8c). Outside of the LC, estimations of D26 were accurate within 10%.

Prestorm SSTs were accurate within the 0.5°C measurement error (Figure 7c), and the differences did not show spatial coherence with the locations of the oceanographic features (Figure 7e). Despite the underestimation of the D26 isotherm in the LC, the maximum magnitude of OHC was accurately diagnosed to be near 150 kJ cm^{-2} (Figure 8c). OHC in the region of the CCE_W was very accurate, while the western WCE was underestimated by satellite due to the center position of the eddy being too far to the southeast.

After Gustav's passage, the D20 isotherm field was accurate in areas with collocated AXBTs and altimetry data (Figure 4d). The region near the CCE_W was not well covered by altimetry such that satellite estimates differed with in situ measurements for D20 by 80 m. Similarly, a large area oriented in the north-south direction along 88°W identified shoaling of 75 m, however this area was not directly observed by the altimeters. Elsewhere in GCW, estimated shoaling of the thermocline by 20 m was accurately determined when near an altimeter track. OHC differences in the poststorm field were directly connected to the underestimations of D26 (Figure 5d) and MLD (Figure 6d) west of the LC. However, OHC estimates were typically accurate to within 15% (Figure 8e).

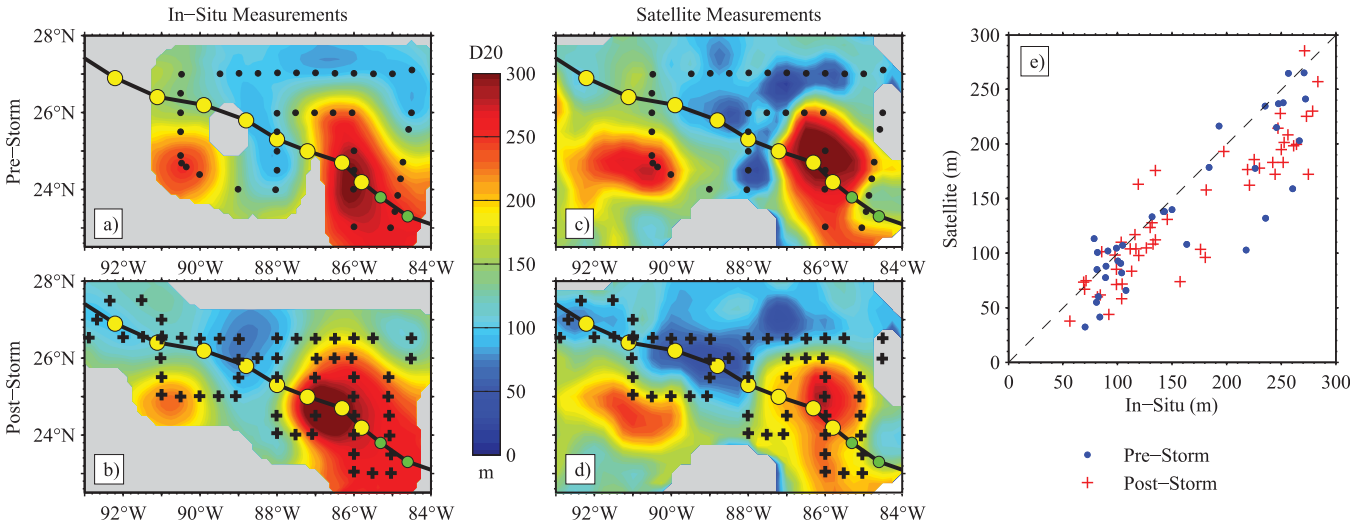

Figure 9. Observations of D20 for Hurricane Ike. (a) In situ prestorm. (b) In situ poststorm. (c) Satellite prestorm. (d) Satellite poststorm. (e) Scatterplot of in situ D20 measurements compared to satellite-derived values for prestorm (blue dot) and poststorm (red +). Observations were taken on 8 September and 15 September for prestorm and poststorm conditions, respectively.

4.2. Hurricane Ike

4.2.1. In Situ Observations

A similar analysis was conducted from the passage of Hurricane Ike where an array of AXBTs was deployed across the forecasted storm track, sampling the LC/WCE complex, CCEs, and a mature WCE to the west. These data confirmed the existence of the closed circulation of the LC bulge (Figure 9a). Maximum depths of D20 and D26 isotherms in the separating WCE were approximately 300 and 210 m, respectively (Figures 9a and 10a). The MLD was still about 60 m due to recent passage of Gustav which did not allow for a new OML to form. Profiles from the western WCE were similar to the LC; however, it did not experience direct atmospheric forcing from Gustav, such that MLDs were typically shallower than in the LC/WCE complex (Figure 11a). OHC values throughout the LC/WCE were consistently near 120 kJ cm^{-2} (Figure 13a). In the CCE_W, the depths of D20 and D26 isotherms were much shallower, reaching only 70 and 30 m, respectively. The OHC values in the CCE were only 40 kJ cm^{-2} which was much lower than the LC due to its shallower thermal structure.

Overlapping AXBT transects along 86°W before and after Ike's passage showed structural changes that occurred in the LC/WCE after Hurricane Ike. D26 shoaled by approximately 30 m in the center of the WCE,

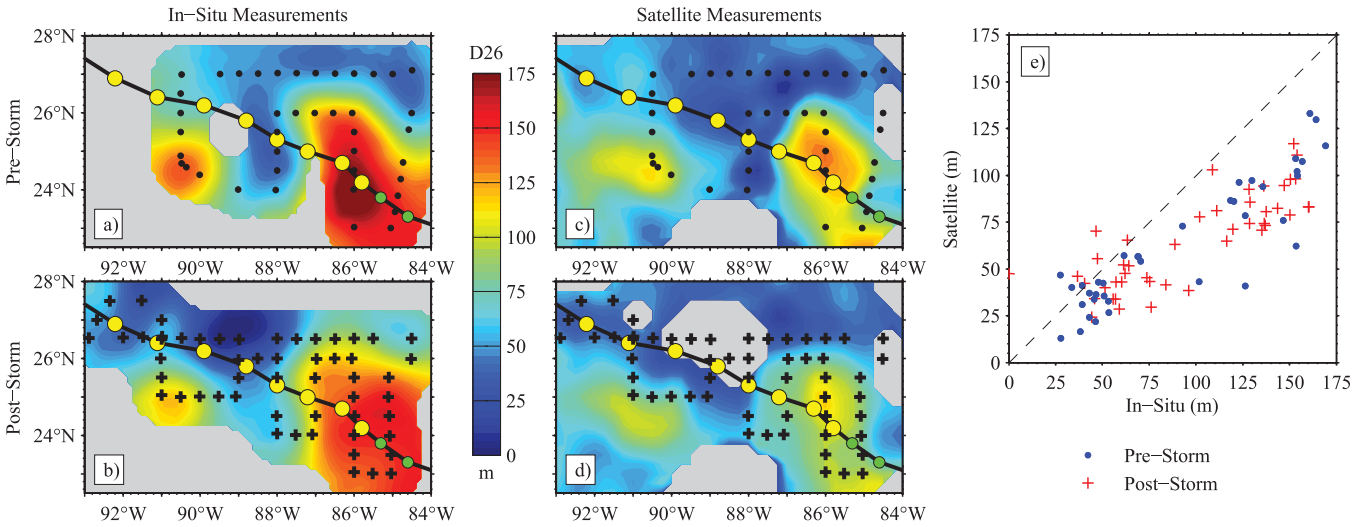

Figure 10. Same as Figure 9, but D26.

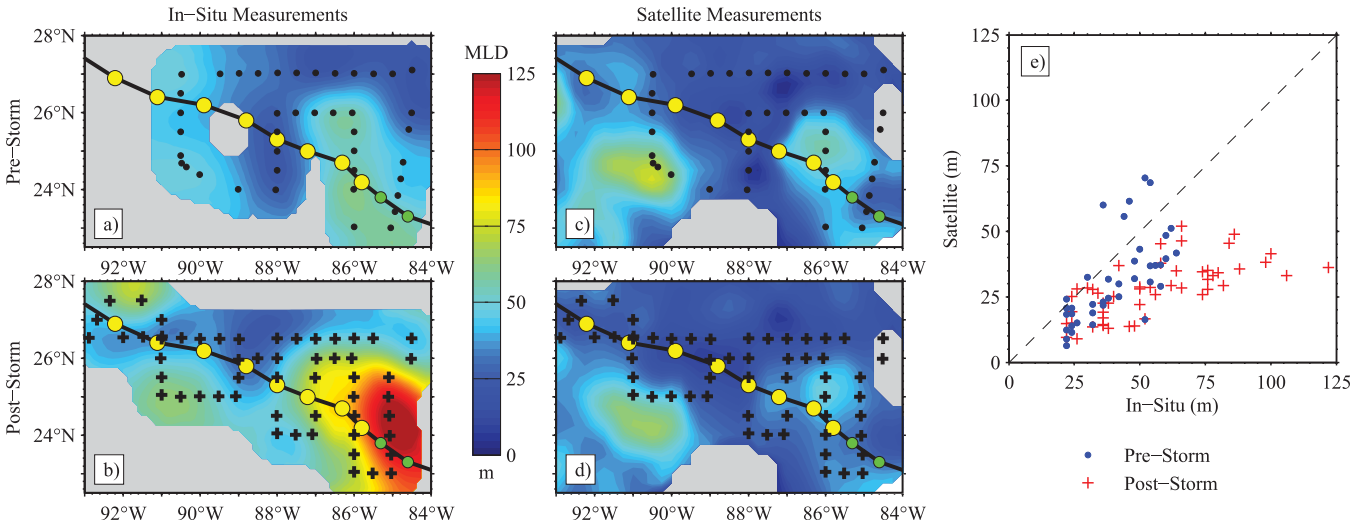

Figure 11. Same as Figure 9, but MLD.

an area where Ike intensified to a Category 2 storm (Figures 9b and 10b). The shoaling was consistent with the scale analysis suggesting isotherm displacement due to Ekman pumping was approximately 20 m. In the WCE eastern region, Ike caused massive deepening of the OML of near 100 m on the right of the storm track (Figure 11b). In the center of the WCE, MLD deepened by 40 m to almost 100 m, while SSTs decreased by 1.5°C. When coupled with the shoaling of D26, OHC decreased by roughly 40 kJ cm^{-2} (Figure 13b).

Directly westward in the CCE$_W$, observations along 88°W suggested deepening of both the D20 and D26 isotherms by 30 and 20 m, respectively (Figures 9b and 10b). The OML deepened by 20 m along this transect, corresponding to a 0.5–1.0°C decrease in SSTs (Figures 11b and 12b). Calculations using pre and poststorm profiles at (24°N, 88°W) indicated entrainment and downwelling each accounted for approximately 10 m of the OML deepening. OHC increased by 20 kJ cm^{-2} in the CCE because of the deepening of the thermal structure and only a small decrease in SSTs (Figures 12b and 13b).

The prestorm flight grid did not capture the core of the CCE, such that full analysis of Ike's effects on the CCE was not comprehensive. The poststorm flight showed the core of the CCE was northwest of the LC/WCE. The CCE was directly under the storm track, and both D20 and D26 shoaled by 40 m with only minimal changes to MLD. SSTs plummeted in this region to the east of the storm track, to as low as 24°C,

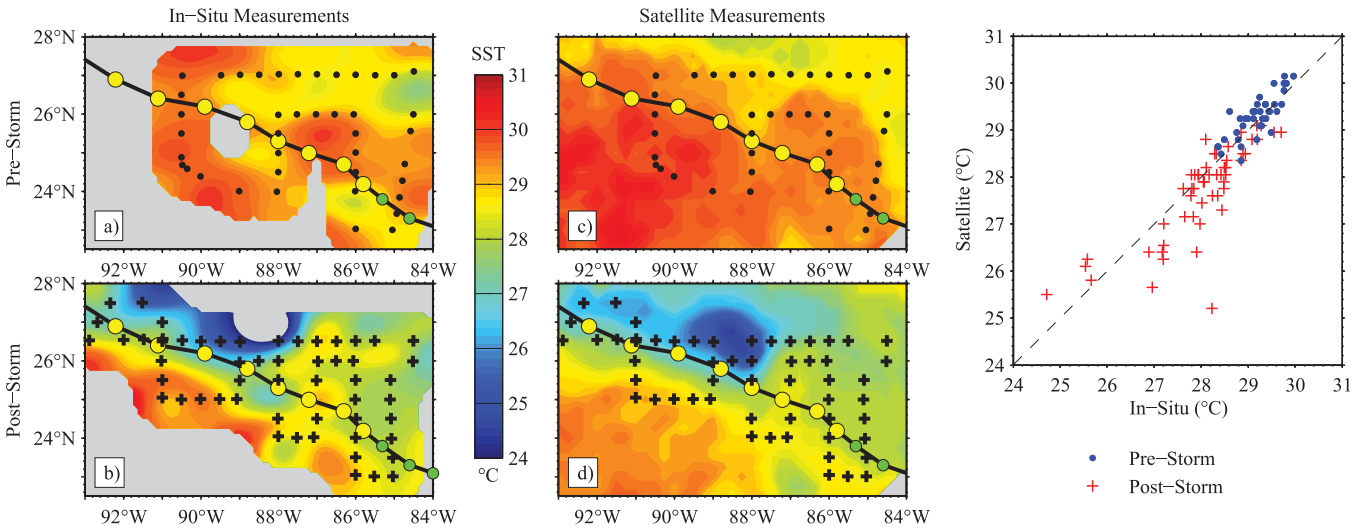

Figure 12. Same as Figure 9, but SST.

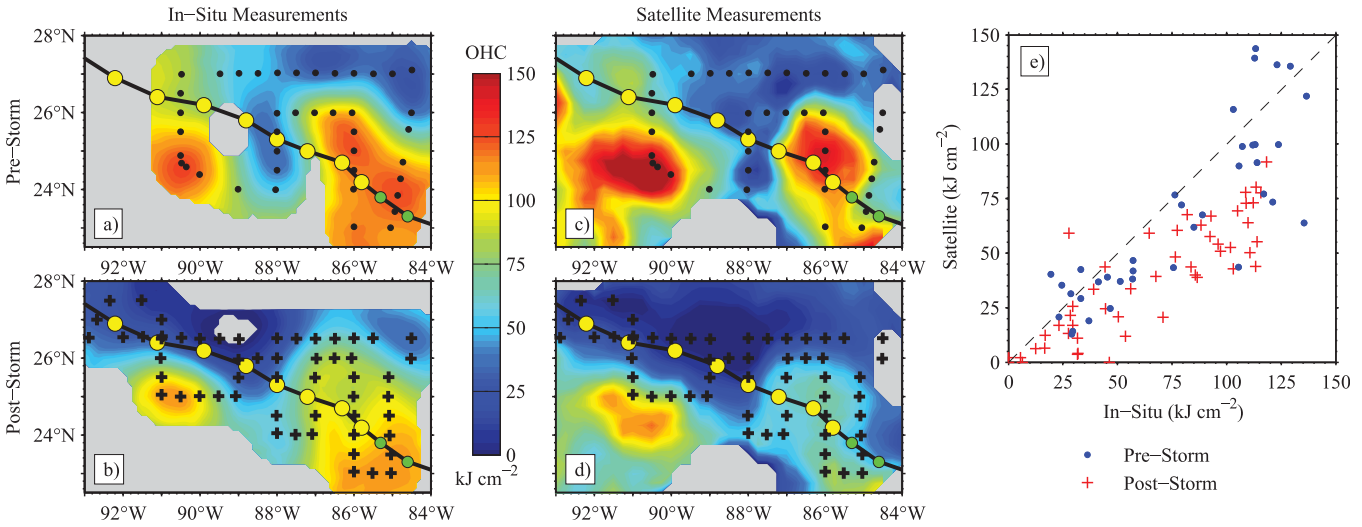

Figure 13. Same as Figure 9, but OHC.

representing a drop of over 4.5°C. This drastic drop eliminated all 40 kJ cm^{-2} of OHC near the CCE core and presumably decreased the enthalpy fluxes.

4.2.2. Satellite Estimations

Altimetry measurements were scarce over the LC/WCE complex prior to Hurricane Ike's passage, such that the center of the LC was not accurately located and the maximum D20 isotherm was overestimated by 25 m (Figures 9c and 9e). Similar to the Gustav case, the gap in altimeter coverage caused poor SSHA estimate over portions of the LC in the southeast extent of the AXBT array (Figure 3c), leading to 100 m and 50 kJ cm^{-2} underestimations of D20 and OHC, respectively (Figures 9e and 13e). The north and west frontal regions of the LC/WCE complex and the center of the western WCE were very accurately located, although D20 depths were overestimated in the WCE by 20 m.

The D26 isotherm was generally underestimated throughout the LC/WCE complex because of the weakly stratified subsurface water mass slightly above 26°C (Figures 10c and 10e) and the inaccuracy of the estimated center of the D20 maximum. The depths of D26 in the CCE were relatively accurate, although the location was inconsistent between the OA of in situ and satellite data. The D26 isotherm in the western WCE was underestimated by over 20 m because an isothermal subsurface layer, similar to one in the LC, was found.

After hurricane passage, the estimated location of the D20 maxima was again too far to the north, although the magnitude of D20 was comparable between in situ and satellite measurements (Figure 7e). The westward extent of the LC/WCE complex was consistent with in situ measurements, such that the accuracy of the satellite estimation was near 10%. Altimetry suggested that the CCE retracted to the north in combination with the formation of a geostrophic baroclinic ridge in the storm's wake [*Geisler*, 1970], but this region was not well covered by altimeters in both the pre and poststorm timeframe. Satellite estimates were consistent with in situ observations in the southern portion of the LC, suggesting shoaling of 20 m. However, to the north, 30 m deepening of D20 was observed where the satellite product suggested shoaling of over 40 m. In the CCE, the overestimated deepening resulted from errors in the prestorm OA, and modest shoaling of D20 in the WCE of 25–40 m was comparable to in situ changes.

The estimated changes between pre and poststorm D26 isotherms mirrored the changes of D20 (Figure 10d). The satellite technique did not depict the 75 m of deepening of the MLD caused by Ike's passage, leading to a satellite overestimation of OHC decrease by 50 kJ cm^{-2} (Figure 13d). The two-layer framework lacks atmospheric forcing, such that the MLD deepening cannot be resolved.

A pronounced cold wake formed behind Hurricane Ike in areas outside of the LC. The southern extent of the satellite-measured SST cooling was too far south, leading to underestimations of OHC in the area (Figure 12d). Due to the large region of satellite SSTs below 26°C, there was a large region with no OHC in the area of the CCE after Ike's passage, which was consistent with in situ measurements. In the LC, the significant

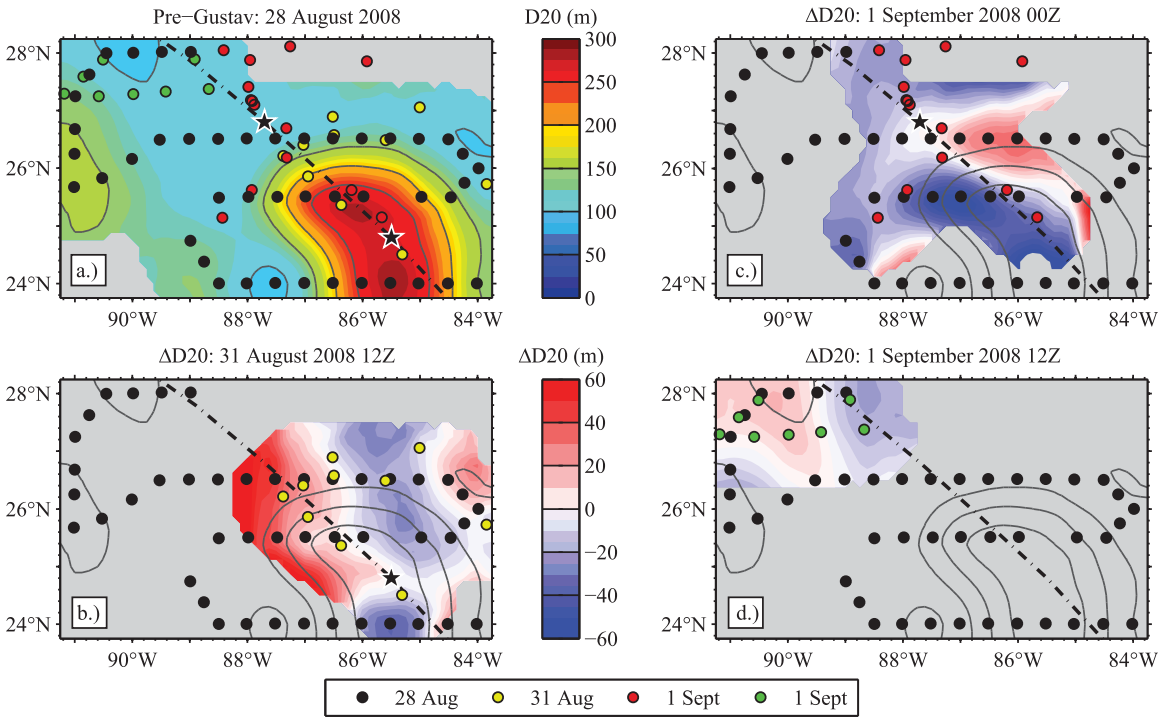

Figure 14. Upwelling response to Hurricane Gustav. (a) Quality-controlled AXBT data points from the four research flights considered in this analysis. Color shading is for the prestorm (28 August) objectively analyzed D20 structure. The storm's track is from the NHC's 6 h best-track data, and the black stars identify storm location during the in-storm flights. (b) Upwelling response during the in storm flight on 31 August at 12Z, defined as the difference in D20 (ΔD20) with respect to prestorm conditions (3 day difference); negative (positive) values of ΔD20 are for upwelling (downwelling) regimes (c) Similar to Figure 14b, but for 1 September at 00Z (3.5 day difference). (d) Similar to Figure 14b, but for 1 September at 12Z (4 day difference). Differences between (Figures 14b and 14c) and (Figures 14c and 14d) represent the 12 h change in the D20 field.

underestimation of MLD deepening (Figures 11d and 11e) led to a 40 kJ cm^{-2} overestimation of the decrease of OHC (Figure 13d). The satellite data correctly identified a region where OHC increased, however the amount of heating was overestimated by 40 kJ cm^{-2}.

5. Forced and Relaxation Stages

5.1. Upwelling Response

Upwelling and downwelling regimes (adiabatic reversible advective processes) can be identified by investigating the fluctuations in D20 because wind-driven vertical mixing (diabatic irreversible turbulent processes) is confined to waters above this depth level in GOM hurricanes [*Price*, 1983*; Jaimes and Shay*, 2009, 2015]. Accordingly, the upwelling responses to Gustav and Ike are investigated in terms of fluctuations in D20, either by computing the difference between prestorm and in-storm D20 structures (the time separation between these structures is from 2 to 4 days), or by computing the difference in D20 structures between consecutive in-storm flights conducted over similar geographic areas with a time separation of 12 h.

Reasonably estimating the rate of upwelling ($\Delta D20/\Delta t$) is only possible for cases of back-to-back in-storm flights. In cases where the prestorm D20 structures are used as a reference, the estimates for ΔD20 are not robust because it is difficult to determine at what point the storm's wind stress began impacting these prestorm structures (although it is likely that this happened within a 24 h time window). Accordingly, the fluctuations of ΔD20 are assumed to occur in a time interval from 12 h (valid for back-to-back in-storm flights) to 24 h. Note that this approach isolates near-inertial processes in the wake of the storm since pre and in-storm (forced stage) D20 structures.

5.1.1. Hurricane Gustav

Before the arrival of Gustav, the LC was fully developed and a recently detached WCE extended to the west (Figure 14a). As Gustav moved over the LC, downwelling of D20 of more than 30 m was measured over the LC's western front respect to prestorm conditions, and moderate upwelling of about 20 m occurred over the LC bulge where horizontal gradients in geostrophic vorticity vanished (Figure 14b). As Gustav moved

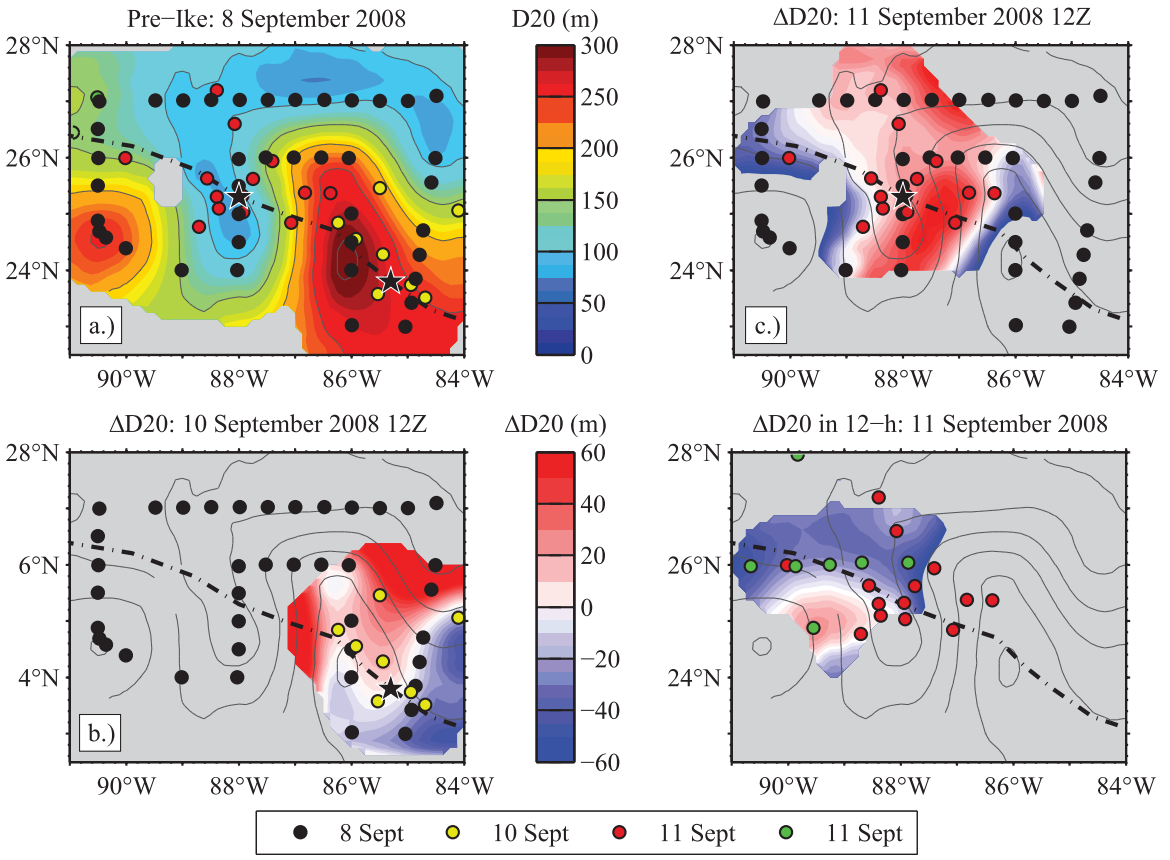

Figure 15. Similar to Figure 14, but for Hurricane Ike. (a) Prestorm D20 values were measured on 8 September 2008. Changes in the D20 field relative to the prestorm observations were calculated for in-storm flights on (b) 10 September and (c) 11 September. (d) The 12 h D20 difference between consecutive in-storm flights on 11 September.

over the LC's northern front, upwelling of 70 m was measured to the left of the track over a 12 h period between reconnaissance flights on 31 August and 1 September 2008 (Figure 14c). The maximum value of $\Delta D20/\Delta t$ was -5.8 m h^{-1} over the upwelling regime. For comparison, maximum downwelling of D20 of 5 m h^{-1} was measured over a 12 h interval during the intensification of tropical storm Isaac into a hurricane over a WCE [*Jaimes and Shay*, 2015]. Gustav begun to weaken to a Category 2 hurricane as it moved over the intense upwelling regime that extended over the LC's NW front.

By contrast, weaker fluctuations in D20 of less than 20 m were measured over quiescent ocean conditions during the time Gustav began making landfall, and a classical structure in upwelling and downwelling regimes was observed [*O'Brien and Reid*, 1967; *Geisler*, 1970; *Price*, 1981], presumably caused just by the structure in the curl of the wind stress (Figure 14d).

5.1.2. Hurricane Ike

One week after the passage of Gustav, and just before the arrival of Ike, the LC retracted and the CCE intensified to the west of the LC (Figure 15a). Quiescent ocean conditions, with shallower D20s than before the passage of Gustav, were measured over the region between the LC and WCE, and over the NE GOM (compare Figures 14a and 15a). As Ike intensified as it traveled across the LC, moderate downwelling of 10–20 m was observed in the LC core (Figure 15b), and intense downwelling of 40 m was measured over the LC frontal regions. Away from the LC's eddy field, a predominant upwelling regime of about 30 m was developed directly below Ike over a 12 h interval on 11 September 2008, where $\Delta D20/\Delta t$ was -2.6 m h^{-1} (Figure 15d).

5.2. Near-Inertial Wake

For both storms, the strongest cooling occurred to the right of the storm track outside of the LC bulge (Figures 7d and 12d). MLDs were relatively shallow and the thermocline was strongly stratified in this area of GCW and a CCE. Cold thermocline water mixed with the thin OML, leading to pronounced SST cooling of 3 and 4.5°C in Hurricanes Gustav and Ike, respectively. Storm-generated currents in the OML are stronger in

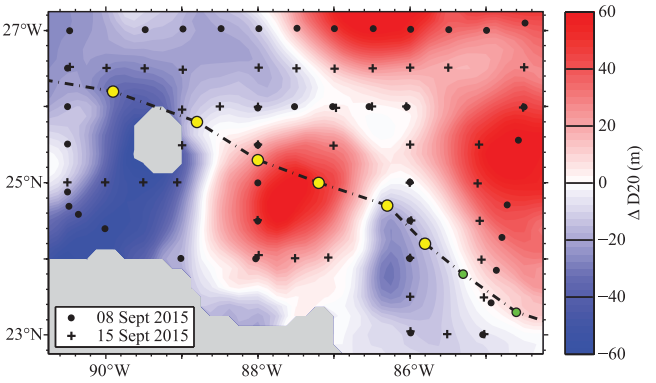

Figure 16. Change to observed D20 field between 8 September and 15 September, with Hurricane Ike's track overlaid.

CCEs than in the LC/WCE complex, which enhances shear-induced mixing at the bottom of the OML [*Price*, 1983; *Jaimes and Shay*, 2009, 2010]. After the forced stage, near-inertial currents persist and can lead to further entrainment and SST cooling. In LC and WCE regimes, however, SST cooling is inhibited because of the deeper depths that tend to be resistive to shear-induced mixing [*Shay and Uhlhorn*, 2008; *Jaimes and Shay*, 2010]. Such physical processes likely occurred during passage of Gustav and Ike, considering SSTs over the LC cooled by less than 1°C.

The near-inertial oceanic response to hurricanes has been well documented in models and observations [*Geisler*, 1970; *Chang and Anthes*, 1978; *Price*, 1983; *Gill*, 1984; *Shay and Elsberry*, 1987; *Shay et al.*, 1998; *Jaimes and Shay*, 2010]. In the wake of Hurricane Ike, there was in situ evidence of a coherent pattern of changes to the prestorm D20 field (Figure 16). The amplitude of the D20 displacement was approximately ±40 m, with a wavelength of 400 km. At this latitude, the inertial period (IP) is 28.7 h, which put the poststorm flight approximately 3–4 IPs after storm passage. Near-inertial currents would still be expected to exist that long after passage based on current decay rates [*Shay and Elsberry*, 1987]. Ike took approximately 30 h to travel between the two D20 anomaly minima, which corresponded with the inertial period and provided support that the anomalies were due to the near-inertial wake.

The near-inertial response was also observed by the array of drifters. Comparing the hourly data from the drifters to the daily data derived using SMARTS revealed the variability of OHC on timescales shorter than 24 h. These fine-scale fluctuations cannot be resolved by the daily satellite product (Figure 17). Surface stress forced near-inertial pumping, which caused D26 isotherms to oscillate by ±8 m (Figure 18a). Outside of periods when SSTs dropped due to mixing and surface fluxes, SSTs remained relatively stable with diurnal cycling of about 0.5°C (Figure 18b). Depending on the phase differences between the near-inertial currents and the diurnal temperature cycle, daily OHC variation was either dampened or enhanced. After an initial decrease of 20 kJ cm^{-2} in the 24 h following deployment, OHC oscillated by ±10 kJ cm^{-2} for several days (Figure 18c).

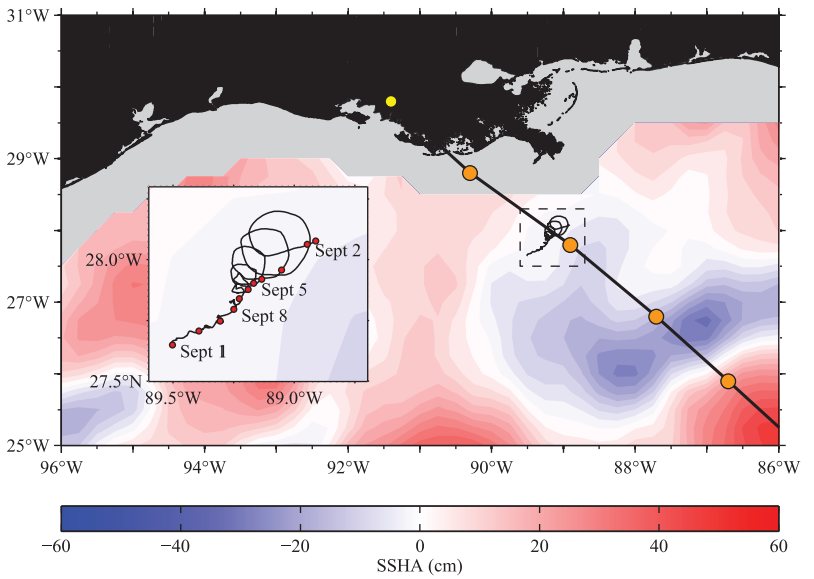

Figure 17. Track of drifter 41615 launched ahead of Hurricane Gustav during the 2008 hurricane season overlaid on SSHA measured by altimetry data. The inset shows the track of the drifter with red circles at 0000Z each day.

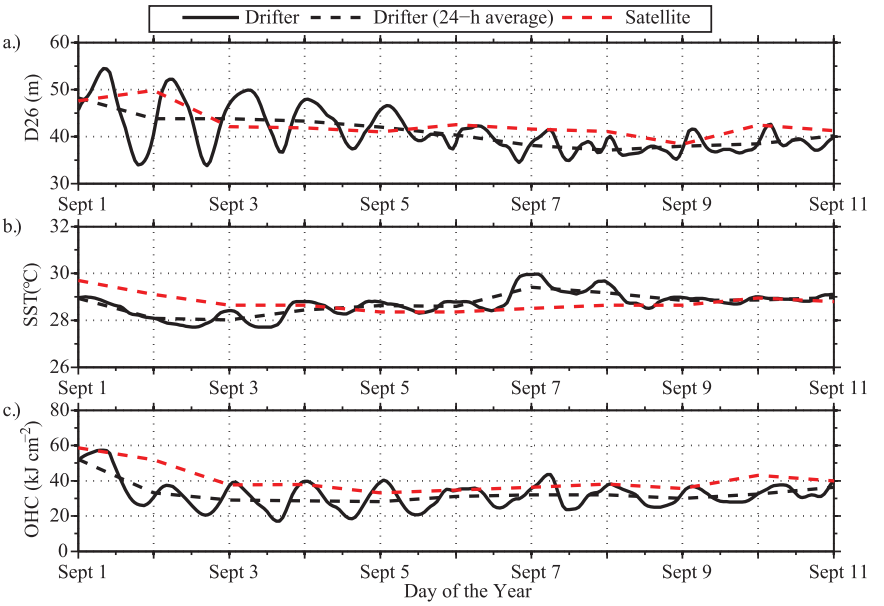

Figure 18. (a) D26, (b) SST, and (c) OHC from drifter 41615 (hourly, solid black; daily average, dashed black) showing diurnal cycles due to near-inertial currents forced by Hurricane Gustav. Satellite data using the SMARTS Climatology (dashed red) is a daily product, and therefore cannot capture the hourly variability.

6. Discussion

The field experiment associated with Hurricanes Gustav and Ike provided a unique opportunity to analyze hurricane impacts on upper ocean thermal structure of mesoscale ocean features during two successive storms. Hurricane Gustav was a relatively compact storm with a small wind field, while Hurricane Ike was much more expansive and had larger impacts on the GOM ocean structure. At the time of passage over the LC, the integrated kinetic energy of hurricane force winds from H*Wind for Gustav and Ike were 16 TJ and 65 TJ, respectively. Additionally, Gustav passed over the GOM much faster, with storm motion averaging about 8 m s^{-1}, compared to about 4 m s^{-1} for Ike. Considering the differences of wind field size and translational speed, it was expected that ocean thermal structure would be more affected by Ike than Gustav. In the LC, MLDs deepened by 30 m in Gustav and over 60 m in Ike. Likewise, MLDs in the CCE deepened twice as much after Ike's passage compared to Gustav.

The satellite estimation of ocean structure using the SMARTS climatology successfully identified the primary oceanographic features during the field campaign. Mean errors and biases from pre, in, and poststorm flights provided insights to the accuracy of the model approach (Table 2). Satellite estimations of the D26 isotherms for the 2008 hurricane season were 10–20% more erroneous than observed in other research campaigns due to the weakly stratified layer beneath the OML just above 26°C. Despite the absolute difference between in situ measurements and satellite estimations of the D26 isotherm, OHC was still relatively accurate, particularly for Hurricane Gustav (RMSD = 23.2 kJ cm^{-2}). However in Hurricane Ike, OHC errors were greater due to the significant underestimations of OML deepening.

Poststorm MLD errors highlighted the shortcomings of the altimetry-based MLD adjustment technique [*Meyers et al*., 2014]. The satellite technique did not capture the extensive deepening of the OML, particularly for Hurricane Ike with its larger wind field. In the two-layer model framework, vertical mixing of upper ocean waters above the D20 isotherm would not significantly affect SSHAs, and therefore the MLD calculation technique did not perform well after a strong wind-forcing event.

Based on the errors in diagnosing MLD deepening, inferences of heat exchange between the atmosphere and ocean must be made with caution when using only satellite-derived OHC data, particularly when two storms cross over the GOM in a small timeframe. In the area of the WCE/LC complex during Hurricane Ike, satellite estimations suggested energy loss in the upper ocean by 50 kJ cm^{-2}, where in situ data determined only 20 kJ cm^{-2} of heat loss occurred. It is expected that MLD, and therefore OHC, will be

Table 2. RMSD Values for D20, D26, MLD, SST, and OHC From the Prestorm and Poststorm AXBT Flight Grids[a]

Gustav	D20 (m)	D26 (m)	MLD (m)	SST (°C)	OHC (kJ/cm^2)
Prestorm (36)	37.6 (1.8)	24.4 (−11.4)	12.4 (−5.7)	0.47 (0.20)	21.1 (−1.6)
Poststorm (38)	38.9 (−6.5)	26.9 (−17.0)	14.1 (−10.7)	0.43 (0.01)	25.6 (−11.1)
All (118)	29.9 (−5.1)	30.4 (−18.0)	18.1 (−12.5)	0.64 (0.31)	23.2 (−5.1)
Ike	D20 (m)	D26 (m)	MLD (m)	SST (°C)	OHC (kJ/cm^2)
Prestorm (33)	33.8 (−12.0)	35.3 (−25.2)	15.2 (−7.3)	0.31 (0.12)	19.7 (−5.7)
Poststorm (31)	43.4 (−31.1)	39.5 (−28.5)	37.8 (−28.0)	0.55 (−0.33)	31.8 (−24.3)
All (129)	46.6 (−22.0)	41.6 (−30.7)	33.0 (−24.1)	0.88 (0.21)	30.4 (−14.7)

[a]Satellite bias is in parentheses. Only AXBTs recorded and processed by University of Miami's Upper Ocean Dynamics Laboratory were used for this analysis.

underestimated by satellite data in most poststorm environments because the wind-forced mixing of the OML is not resolved in the two-layer model .

7. Concluding Remarks

Neither Gustav nor Ike experienced rapid deepening while traversing the LC or WCE. Gustav's intensification was hindered by unfavorable synoptic conditions, whereas Ike underwent an eyewall replacement cycle over the LC. The warm ocean supported the formation of the secondary eyewall, which vastly expanded the hurricane wind field and total kinetic energy.

A key finding of this study is that the structure of the upwelling response is not just a function of the curl of the wind stress, since the background geostrophic flow significantly impacted the structure in upwelling and downwelling responses to both Gustav and Isaac. Intense downwelling regimes were observed over the LC front, similar to downwelling regimes observed over WCEs during Hurricanes Rita (2005) and Isaac (2012) [*Jaimes and Shay*, 2009, 2015]. These downwelling regimes are associated with wind-driven vortex stretching and ensuing eddy intensification.

The combined effect of Hurricanes Gustav and Ike caused the OML to deepen by 100 m over the weakly stratified LC. As expected, the SST cooling in the wake of both storms was more pronounced over GCW (−4 to −6°C) than over the LC/WCE complex (−1 to −2°C). The lower SSTs and 10–20 m of upwelling from Ekman pumping acted to decrease OHC over most of the domain; however, OHC increased in convergence zones of the near-inertial wake.

A drawback to the two-layer model was the lack of wind-forced mixing, leading to errors in the poststorm analysis. While altimeters could detect changes to the SSHA field caused by mass transport (i.e., the internal wake field), modifications to upper ocean temperature profiles caused by mixing at the base of the OML is not explicit in the two-layer model. The ocean state had not equilibrated after the passage of Hurricane Gustav, such that the satellite estimates of OHC ahead of Hurricane Ike were overestimated in the LC core.

Analysis of high temporal resolution drifter data revealed model errors for the satellite estimates after strong wind-forcing events. Once-daily satellite estimates of ocean thermal structure were calculated; however, the drifter data showed diurnal variability of over 30% of the mean value which led to periodic measurement errors (Figures 12a and 12c). An open question is whether the error is the same for cyclonic, anticyclonic, and quiescent flow. The kinematics of near-inertial motions is impacted by stratification and vorticity of the background ocean, such that this error could be smaller (larger) over WCE (CCE) where near-inertial motions are weaker (stronger).

This study highlighted the importance of synchronized in situ and satellite measurements for complete and accurate characterization of the ocean thermal structure in the hurricane environment. Satellite estimates provided full coverage of the Atlantic hurricane basin, but in situ measurements were necessary to identify features not resolvable by the two-layer model, such as the thermocline temperature gradient and intense OML deepening. Additionally, the in situ measurements serve as ground truth to ensure satellite estimates are producing realistic features of appropriate magnitudes. Observations of ocean currents in the hurricane environment are essential to calculate vertical shear, upwelling, and mixing. The in situ data are needed to improve estimates of the ocean response from satellite products; to provide accurate depictions of ocean features needed to improve operational statistical intensity forecasting at NHC; and to improve parameterizations of vertical mixing over the stratified ocean in numerical models.

Acknowledgments
Parties interested in obtaining satellite-derived data used in this study for Hurricanes Gustav and Ike should contact Nick Shay (nshay@rsmas.miami.edu) to register for access to the University of Miami's Upper Ocean Dynamics Laboratory (UODL) data archive (http://www.rsmas.miami.edu/groups/upper-ocean-dynamics/research/ocean-heat-content/data-archive/#). The in situ AXBT data are processed with proprietary software of the UODL and cannot be openly shared, however AXBT data are available through the HRD (http://www.aoml.noaa.gov/hrd/data_sub/hurr2008.html). NOAA/AOML/PHOD (Rick Lumpkin) generously provided the processed drifter data The research team gratefully acknowledge support from NASA Hurricane Science Program (NASA Award NNX09AC47G), NOAA Joint Hurricane Testbed (NOAA grant: NA17RJ1226) program, and NOAA/NESDIS. The project continues to be grateful to the NOAA Aircraft Operation Center (Jim McFadden) who make it possible to acquire high-quality data during hurricanes through the Hurricane Forecast Improvement Project (HFIP) and the collaborative ties with NOAA's Hurricane Research Division directed by Frank Marks at AOML and NOAA's Environmental Modeling Center directed by Hendrick Tolman at NCEP.

References

Berg, R. (2009), Tropical cyclone report: Hurricane Ike, Natl. Hurricane Cent., Report no. AL092008, 55 pp., Miami, Fla.
Beven, J. L., and T. B. Kimberlain (2009), Tropical cyclone report: Hurricane Gustav, Natl. Hurricane Cent., Report no. AL072008, 38 pp., Miami, Fla.
Boyd, J. (1987), Improved depth and temperature conversion equations for Sippican AXBTs, *J. Atmos. Oceanic Technol.*, *4*, 545–551.
Chang, S. W., and R. A. Anthes (1978) Numerical simulations of the ocean's nonlinear, baroclinic response to translating hurricanes, *J. Phys. Oceanogr.*, *8*, 468–480.
D'Asaro, E. A. (1985), Upper ocean temperature structure, inertial currents, and Richardson numbers observed during strong meteorological forcing, *J. Phys. Oceanogr.*, *15*, 943–962.
Emanuel, K. A. (1999), Thermodynamic control of hurricane intensity, *Nature*, *401*, 665–669.
Fisher, E. L. (1958), Hurricanes and the sea surface temperature field, *J. Meteorol.*, *15*, 328–333.
Geisler, J. E. (1970), Linear theory of the response of a two layer ocean to a moving hurricane, *Geophys. Fluid Dyn.*, *1*, 249–272.
Gentemann, C. L., C. J. Donlon, A. Stuart-Menteth, and F. J. Wentz (2003), Diurnal signals in satellite sea surface temperature measurements, *Geophys. Res. Lett.*, *30*(3), 1140, doi:10.1029/2002GL016291.
Gentemann, C. L., F. J. Wentz, C. A. Mears, and D. K. Smith (2004), In situ validation of tropical rainfall measuring mission microwave sea surface temperatures, *J. Geophys. Res.*, *109*, C04021, doi:10.1029/2003JC002092.
Gill, A. E. (1984), On the behavior of internal waves in the wakes of storms, *J. Phys. Oceanogr.*, *14*, 1129–1151.
Halliwell, G., L. K. Shay, S. D. Jacob, O. Smedstad, and E. Uhlhorn (2008), Improving ocean model initialization for coupled tropical cyclone forecast models using GODAE nowcasts. *Mon. Weather Rev.*, *136* (7), 2576–2591, doi:10.1175/2007MWR2154.1.
Jacob, S. D., L. K. Shay, A. J. Mariano, and P. G. Black (2000), The 3-D oceanic mixed-layer response to Hurricane Gilbert, *J. Phys. Oceanogr.*, *30*(6), 1407–1429.
Jaimes, B., and L. K. Shay (2009), Mixed layer cooling in mesoscale oceanic eddies during hurricanes Katrina and Rita, *Mon. Weather Rev.*, *137*, 4188–4207, doi:10.1175/2009MWR2849.1.
Jaimes, B., and L. K. Shay (2010), Near-inertial wave wake of hurricanes Katrina and Rita over mesoscale oceanic eddies, *J. Phys. Oceanogr.*, *40*, 1320–1337, doi:10.1175/2010JPO4309.1.
Jaimes, B., and L. K. Shay (2015), Enhanced wind-driven downwelling flow in warm oceanic eddy features during the intensification of tropical cyclone Isaac (2012): Observations and theory, *J. Phys. Oceanogr.*, *45*, 1667–1689, doi:10.1175/JPO-D-14-0176.1.
Jaimes, B., L. K. Shay, and E. W. Uhlhorn (2015), Enthalpy and momentum fluxes during Hurricane Earl relative to underlying ocean features, *Mon. Weather Rev.*, *143*, 111–131, doi:10.1175/MWR-D-13-00277.1.
Landsea, C. W., and J. L. Franklin (2013), Atlantic hurricane database uncertainty and presentation of a new database format, *Mon. Weather Rev.*, *141*, 3576–3592, doi:10.1175/MWR-D-12-00254.1.
Leipper, D. F. (1967), Observed ocean conditions and Hurricane Hilda, *J. Atmos. Sci.*, *24*, 182–196.
Lin, I.-I., C.-C. Wu, K. A. Emanuel, I.-H. Lee, C.-R. Wu, and I.-F. Pun (2005), The interaction of super typhoon Maemi (2003) with a warm ocean eddy, *Mon. Weather Rev.*, *133*, 2635–2649.
Maclay, K. S., M. DeMaria, and T. H. V. Haar (2008), Tropical cyclone inner-core kinetic energy evolution, *Mon. Weather Rev.*, *136*, 4882–4898, doi:10.1175/2008MWR2268.1.
Mainelli, M., M. DeMaria, L. K. Shay, and G. Goni (2008), Application of oceanic heat content estimation to operational forecasting of recent Atlantic Category 5 hurricanes, *Weather Forecast*, *23*, 3–16, doi:10.1175/2007WAF2006111.1.
Mariano, A. J., and O. B. Brown (1992), Efficient objective analysis of dynamically heterogeneous and nonstationary fields via the parameter matrix, *Deep Sea Res., Part A*, *39*, 1255–1271.
Meyers, P. C. (2011), Development of the systematically merged Atlantic regional temperature and salinity climatology, MS thesis, Div. of Meteorol. and Phys. Oceanogr., Rosenstiel Sch. of Mar. and Atmos. Sci., Univ. of Miami, Miami, Fla.
Meyers, P. C., L. K. Shay, and J. K. Brewster (2014), Development and analysis of the systematically merged Atlantic regional temperature and salinity climatology for oceanic heat content estimates, *J. Atmos. Oceanic Technol.*, *31*, 131–149, doi:10.1175/JTECH-D-13-00100.1.
O'Brien, J. J., and R. O. Reid (1967), The non-linear response of a two-layer, baroclinic ocean to a stationary, axially-symmetric hurricane: Part I. Upwelling induced by momentum transfer. *J. Atmos. Sci.*, *24*, 197–207.
Palmen, E. (1948), On the formation and structure of tropical cyclones. *Geophysika*, *3*, 26–38.
Powell, M. D., S. H. Houston, L. R. Amat, and N Morisseau-Leroy (1998), The HRD real-time hurricane wind analysis system, *J. Wind Eng. Ind. Aerodyn.*, *77,78*, 53–64.
Price, J. F. (1981), Upper ocean response to a hurricane, *J. Phys. Oceanogr.*, *11*, 153–175.
Price, J. F. (1983), Internal wave wake of a moving storm. Part I. scales, energy budget and observations, *J. Phys. Oceanogr.*, *13*, 949–965.
Sanford, T. B., P. G. Black, J. R. Haustein, J. W. Feeney, G. Z. Forristall, and J. F. Price (1987), Ocean response to a hurricane. Part I: Observations, *J. Phys. Oceanogr.*, *17*, 2065–2083.
Shay, L. K., and R. L. Elsberry (1987), Near-inertial ocean current response to Hurricane Frederic, *J. Phys. Oceanogr.*, *17*, 1249–1269.
Shay, L. K., and E. Uhlhorn (2008), Loop current response to hurricanes Isidore and Lili, *Mon. Weather Rev.*, *137*, 3248–3274, doi:10.1175/2007MWR2169.1.
Shay, L. K., S. W. Chang, and R. L. Elsberry (1990), Free surface effects on the near-inertial ocean current response to a hurricane, *J. Phys. Oceanogr.*, *20*, 1405–1424.
Shay, L. K., P. G. Black, A. J. Mariano, J. D. Hawkins, and R. L. Elsberry (1992), Upper ocean response to hurricane Gilbert, *J. Geophys. Res.*, *97*, 20,227–20,248.
Shay, L. K., A. J. Mariano, S. D. Jacob, and E. H. Ryan (1998), Mean and near-inertial ocean current response to hurricane Gilbert, *J. Phys. Oceanogr.*, *28*, 858–889.
Shay, L. K., G. J. Goni, and P. G. Black (2000), Effects of a warm oceanic feature on Hurricane Opal, *Mon. Weather Rev.*, 125(5), 1366–1383.
Shay, L. K., B. Jaimes, J. K. Brewster, P. Meyers, E. C. McCaskill, E. Uhlhorn, F. Marks, G. R. Halliwell, Jr., O. M. Smedstad, and P. Hogan (2011), Airborne ocean surveys of the Loop Current complex from NOAA WP-3D in support of the Deepwater Horizon oil spill, in *Monitoring and Modeling the Deepwater Horizon Oil Spill: A Record-Breaking Enterprise, Geophys. Monogr. Ser.*, vol. 195, edited by Y. Liu et al., pp. 131–151, AGU, Washington, D. C., doi:10.1029/2011GM001101.
Wada, A. and J. C. L. Chan (2008), Relationship between typhoon activity and upper ocean heat content, *Geophys. Res. Lett.*, *35*, L17603, doi:10.1029/2008GL035129.